

Electronic Supplementary Information (ESI) for

Nanochannel-Based {BaZn}-Organic Framework for Catalytic Activity on Cycloaddition Reaction of Epoxides with CO₂ and Deacetalization-Knoevenagel Condensation

Hongxiao Lv,^a Liming Fan,^a Hongtai Chen,^a Xiutang Zhang,^{*a} and Yanpeng Gao^{*b}

^aDepartment of Chemistry, College of Science, North University of China, Taiyuan 030051, P.R. China. E-mail: xiutangzhang@163.com.

^bCollege of Chemical Engineering, Ordos Institute of Technology, Ordos, Inner Mongolia, China 017000. E-mail: gaoyanpeng0000001@163.com.

Table of Contents

Experimental Section

Table S1. Crystallographic data and refinement parameters of **NUC-51**.

Table S2. Selected bond lengths and angles.

Table S3. The detailed structure comparisons among complexes **NUC-27** and **NUC-51**.

Table S4. Published Zn or Ba-based MOFs' catalytic effect of cycloaddition reaction.

Table S5. The molecular sizes of epoxides and corresponding products of cycloaddition reaction.

Table S6. The molecular sizes of reactants and corresponding products of deacetalization-Knoevenagel condensation reaction.

Table S7. The cation exchange between tetrabutylammonium cations (TBA^+) and dimethylamine cations (DMA^+) in **NUC-51a**.

Fig. S1. The inner surface environment in **NUC-51**.

Fig. S2. The PXRD patterns of as-synthesized **NUC-51** and simulation.

Fig. S3. The SEM image of **NUC-51**.

Fig. S4. The PXRD patterns of **NUC-51** sample under water treatment.

Fig. S5. Energy dispersive spectroscopy (EDS) elemental mappings of **NUC-51** sample for C, N, O, Ba and Zn.

Fig. S6. The FT-IR spectrum of **NUC-51** and **NUC-51a'**.

Fig. S7. The TGA curves of **NUC-51** and **NUC-51a**.

Fig. S8. The PXRD patterns of **NUC-51** at variable temperatures.

Fig. S9. The catalytic efficiency of **NUC-51a** and **NUC-51a'** for cycloaddition reaction.

Fig. S10. The PXRD patterns of **NUC-51a** and **NUC-51a'** after cycloaddition reaction and deacetalization-Knoevenagel condensation reaction.

Fig. S11. The PXRD patterns of **NUC-51a** and simulation.

Fig. S12. N_2 adsorption and desorption isotherms of **NUC-51a** at 77 K.

Fig. S13. CO_2 sorption isotherms of **NUC-51a** at 273 and 298 K.

Isosteric Heat Calculation.

Fig. S14. CO_2 adsorption heat calculated by the virial equation of **NUC-51a**.

Yield Calculation Based on the GC-MS Analysis.

Fig. S15. ^1H NMR spectrum of propylene carbonate.

Fig. S16. ^1H NMR spectrum of 4-fluoro-1,3-dioxolan-2-one.

Fig. S17. ^1H NMR spectrum of 4-chloro-1,3-dioxolane-2-one.

Fig. S18. ^1H NMR spectrum of 4-ethyl-1,3-dioxolan-2-one.

Fig. S19. ^1H NMR spectrum of 4-(trifluoro)-1,3-dioxolane-2-one.

Fig. S20. ^1H NMR spectrum of 4-vinyl-1,3-dioxolan-2-one.

Fig. S21. ^1H NMR spectrum of 4-phenyl-1,3-dioxolan-2-one.

Fig. S22. Recyclability study (five cycles) for catalytic activities of **NUC-51a** in cycloaddition reaction of styrene oxide with CO_2 .

Fig. S23. The PXRD patterns of **NUC-51a** after recycled cycloaddition reaction.

- Fig. S24.** Evidence of heterogeneous nature of **NUC-51a** in the cycloaddition reaction.
- Fig. S25.** The catalytic mechanism of cycloaddition reaction of epoxides with CO₂.
- Fig. S26.** ¹H NMR spectrum of 2-[(4-nitrophenyl) methylidene] propanedinitrile.
- Fig. S27.** ¹H NMR spectrum of 2-[(4-fluorophenyl)methylidene] propanedinitrile.
- Fig. S28.** ¹H NMR spectrum of 2-[(4-bromophenyl)methylidene] propanedinitrile.
- Fig. S29.** ¹H NMR spectrum of 2-(phenylmethylidene)propanedinitrile.
- Fig. S30.** ¹H NMR spectrum of 2-[(3,4-dimethoxyphenyl)methylidene]propanedinitrile.
- Fig. S31.** ¹H NMR spectrum of 2-[(3,4,5-trimethoxyphenyl)methylidene]propanedinitrile.
- Fig. S32.** ¹H NMR spectrum of 2-[(4-methylphenyl)methylidene]propanedinitrile.
- Fig. S33.** ¹H NMR spectrum of 2-[(3,4-dimethylphenyl)methylidene]propanedinitrile.
- Fig. S34.** ¹H NMR spectrum of 2-[(anthracen-9-yl)methylidene]propanedinitrile.
- Fig. S35.** ¹H NMR spectrum of 2-[[4-(3,5-dimethylphenoxy)phenyl]methylidene] ropanedinitrile.
- Fig. S36.** Recyclability study for catalytic activities of **NUC-51a** in deacetalization-Knoevenagel reaction.
- Fig. S37.** The PXRD patterns of **NUC-51a** after recycled deacetalization-Knoevenagel reaction.
- Fig. S38.** Evidence of heterogeneous nature of **NUC-51a** in the deacetalization-Knoevenagel reaction.
- Fig. 39.** Plausible reaction mechanism of deacetalization-Knoevenagel reaction catalyzed by **NUC-51a**.
- Fig. 40.** Two dimensional molecular sizes of deacetalization-Knoevenagel reaction reactants and products.
- Reference**

Experimental Section

Materials and General Methods

Thermogravimetric analyses (TGA) from room temperature to 800 °C were carried out by a NETZSCH STA 449 F3 thermogravimetric analyzer under air flow at a 10 °C/min ramp rate. IR spectrum in the range of 500-4000 cm⁻¹ was collected on a Nicolet 740 FT-IR spectrometer. Element analysis (EA) for C, N, and H was monitored on the EA 1110 element analyzer of CE instrument. Powder X-ray diffraction (PXRD) was collected for 2θ values (5~30°) on X-Pert pro diffractometer with Cu-K α radiation. The N₂ (77K) and CO₂ (273K and 298K) adsorption-desorption isotherms were performed on an ASAP 2020 Plus instrument. Inductively coupled plasma (ICP) measurements were analyzed on an IRIS Advantage spectrometer equipped with a CCD detector and Ar plasma covering 175-785 nm range. Gas chromatography mass spectrometry (GC-MS) analyses were performed on a time-of-flight Thermo Fisher Trace ISQ GC/MS instrument. ¹H NMR spectra were recorded on a JEOL-ECX 500 FT (400 MHz) instrument with *n*-dodecane as the internal standard.

X-ray crystallography

A summary of crystallographic data, refinement parameter and bond lengths and angles for **NUC-51** were given in Table S1 and S2. The diffraction intensity data for **NUC-51** was obtained at 296(2) K by using a Bruker Smart-APEX II CCD area detector (Mo-K α radiation, $\lambda = 0.071073$ nm) with graphite-monochromated radiation. The data integration and reduction were processed with SAINT software. The reflection data were consequently corrected for empirical absorption corrections and Lorentz and polarization effects. The structure was solved by direct methods and refined by full-matrix least-squares with the SHELXL package. All non-hydrogen atoms were refined anisotropically, until convergence was attained. Hydrogen atoms except those on water molecules were generated geometrically with fixed isotropic thermal parameters, and included in the structure factor calculations. The block of SQUEEZE in PLATON was employed to eliminate the highly disordered solvent molecular. Further details on the crystal structure investigations may be obtained from the Cambridge Crystallographic Data Centre, with the depository number CCDC-2072307 for **NUC-51**.

Table S1. Crystallographic data and refinement parameters of **NUC-51**.

Complex	NUC-51
Formula	C ₂₉ H ₁₁ BaNO ₁₃ Zn
Mr	784.10
Crystal system	trigonal
Space group	R-3m
a (Å)	48.046(10)
b (Å)	48.046(10)
c (Å)	13.469(3)
α (°)	90
β (°)	90
γ (°)	120
V(Å ³)	26926(13)
Z	18
Dcalcd(g·cm ⁻³)	0.870
μ(mm ⁻¹)	5.885
GOF	1.033
R ₁ [I>2σ(I)] ^a	0.0541
wR ₂ [I>2σ(I)] ^b	0.1484
R ₁ ^a (all data)	0.0664
wR ₂ ^b (all data)	0.1566
R _{int}	0.1318

$$^a R_1 = \sum \left| \frac{|F_o| - |F_c|}{|F_o|} \right| \cdot \quad ^b wR_2 = \left[\frac{\sum w(|F_o|^2 - |F_c|^2)^2}{\sum w(F_o^2)^2} \right]^{1/2}$$

Table S2. Selected bond lengths and angles.

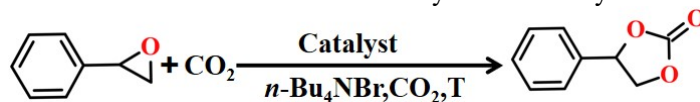
Selected bond lengths/Å					
Ba1-O5 ¹	2.338(5)	Ba1-O2 ²	2.307(4)	Ba1-O2	2.307(4)
Ba1-O4 ³	2.422(4)	Ba1-O4 ⁴	2.422(4)	Ba1-O3 ³	2.473(4)
Ba1-O3 ⁴	2.473(4)	Ba1-O1W	2.419(6)	Zn1-O7 ⁵	1.928(5)
Zn1-O1 ²	1.962(5)	Zn1-O1	1.962(5)	Zn1-O6 ¹	1.923(5)
Selected angles/°					
O5 ¹ -Ba1-O4 ²	75.54(1)	O5 ¹ -Ba1-O4 ³	75.53(1)	O5 ¹ -Ba1-O3 ²	125.75(1)
O5 ¹ -Ba1-3 ³	125.7(1)	O5 ¹ -Ba1-O1W	148.9(2)	O2-Ba1-O5 ¹	79.54(2)
O2 ⁴ -Ba1-O5 ¹	79.53(2)	O2 ⁴ -Ba1-O2	87.5(2)	O24-Ba1-O4 ³	91.80(2)
O2 ⁴ -Ba1-O4 ²	154.7(2)	O2-Ba1-O4 ²	91.81(2)	O2-Ba1-O4 ³	154.76(2)
O2-Ba1-O3 ²	88.82(2)	O2 ⁴ -Ba1-O3 ²	153.20(2)	O2-Ba1-O3 ³	153.20(2)
O2 ⁴ -Ba1-O3 ³	88.81(2)	O2-Ba1-O1W	78.11(2)	O2 ⁴ -Ba1-O1W	78.10(2)
O4 ² -Ba1-O4 ³	78.3(3)	O4 ² -Ba1-O3 ³	102.53(2)	O4 ² -Ba1-O3 ²	51.87(2)
O4 ³ -Ba1-O3 ³	102.5(2)	O3 ² -Ba1-O3 ³	82.7(3)	O1W-Ba1-O4 ³	126.39(2)
O1W-Ba1-O4 ²	126.4(2)	O1W-Ba1-O3 ²	75.16(2)	O1W-Ba1-O3 ³	75.16(2)
O2 ⁴ -Ba1-O4 ³	91.80(2)	O7 ⁵ -Zn1-O1	103.97(1)	O1 ⁴ -Zn1-O1	113.9(3)
O6 ¹ -Zn1-O7 ⁵	101.3(2)	O6 ¹ -Zn1-O1 ⁴	115.61(1)	O6 ¹ -Zn1-O1	115.61(1)
O7 ⁵ -Zn1-O1 ⁴	103.9(1)				

Symmetry codes: ¹-y+2/3,x-y+1/3,+z+1/3; ²-x+2/3,y-x+1/3,-z+4/3; ³y-1/3,y-x+1/3,-z+4/3; ⁴+y-x,+y,+z; ⁵y-1/3,y-x+1/3,-z+1/3; ⁶-y+1,-x+1,+z; ⁷x-y+2/3,x+1/3,-z+1/3; ⁸y-x+1/3,-x+2/3,z-1/3; ⁹x-y+2/3,x+1/3,-z+4/3.

Table S3. The detailed structure comparisons among complexes **NUC-27** and **NUC-51**.

Complex	NUC-27	NUC-51
Unit cell system	monoclinic system	trigonal system
Space group	<i>P21/n</i>	<i>R-3m</i>
Molecular formula	$\{[\text{Ba}_3\text{Zn}_4(\text{TDP})_2(\text{HCO}_2)_2(\text{OH}_2)_2] \cdot 7\text{DMF} \cdot 4\text{H}_2\text{O}\}_n$	$\{[(\text{CH}_3)_2\text{NH}_2]_2[\text{BaZn}(\text{TDP})(\text{H}_2\text{O})] \cdot \text{DMF} \cdot 5\text{H}_2\text{O}\}_n$
Void volume occupancy	58.8%	62.1%
Carboxyl coordination mode	$\mu_2\text{-}\eta^1\text{:}\eta^1$	$\mu_1\text{-}\eta^0\text{:}\eta^1$; $\mu_1\text{-}\eta^1\text{:}\eta^1$; $\mu_2\text{-}\eta^1\text{:}\eta^1$
in TDP⁶⁻		
SBU	$[\text{BaZn}_2(\text{CO}_2)_6]$ and $[\text{BaZn}(\text{CO}_2)_3(\text{OH}_2)]$	$[\text{BaZn}(\text{CO}_2)_6(\text{H}_2\text{O})]$
Zn Coordination number	tetra-coordination	tetra-coordination
Ba Coordination number	hexa- and tetra-coordinated	eight-coordination
3D architectures	3-nodal 4-connected 2D sheet	5-connected nodes <i>fn</i> g-type 3D structure
Point (Schläfli) symbol	$\{3.6^4.7\}_4\{3^2.6^2.7^2\}$	$\{4^6.6^4\}$
Synthetic conditions	3 mL DMF, 3 mL EtOH, 1.5 mL H ₂ O and 0.1 mL 10% HNO ₃ ; Heated at 130 °C for 72h	3 mL DMF, 3 mL EtOH, 4 mL H ₂ O and 0.1 mL 10% HNO ₃ ; Heated at 130 °C for 72h

Table S4. Published Zn or Ba-based MOFs' catalytic effect of cycloaddition reaction.



MOF	Catalyst (mmol)	<i>n</i> -Bu ₄ NBr (mmol)	Temperature (°C)	Pressure (atm)	Time (h)	Yield (%)	TON ^a	TOF ^b (h ⁻¹)	Ref.
Zn-MOF-74	0.06	0.075	80	1	6	70	58.3	9.7	S1
Zn-MOF-184	0.06	0.075	80	1	6	82	68.3	11.4	S1
PNU-21	0.15	0.075	80	4	8	66	110	13.75	S2
Ba-MOF	0.1	0.4	25	1	48	19.8	39.6	0.83	S3
ZnMOF-1-NH ₂	0.2	0.5	80	8	8	88	58	7.3	S4
NUC-27	0.4	1.0	60	1	8	98	45	5.6	S5
NUC-21	0.2	1.0	60	1	6	92	46	7.6	S6
NUC-30	0.2	1.0	60	10	12	92	92	7.7	S7
NUC-51	0.2	1.0	55	1	6	97.2	121.3	16.2	Our

^aTON= turnover number (defined as moles of the yielded product per mole of the catalyst per hour); ^bTOF = turnover frequency;

Molecular formula:

Zn-MOF-74: Zn₂ (2,5-dihydroxyterephthalic acid);

Zn-MOF-184: Zn₂ (4,4'-(ethyne-1,2-diyl)bis(2-oxido-Benzoate));

PUN-21: [Zn₂(H₂O)(stdb)₂(5H-Ade)(9H-Ade)₂]_n;

Ba-MOF: {[Ba₂(BDPO)(H₂O)]·DMA}_n;

ZnMOF-1-NH₂: {[Zn(ATA)(L)·H₂O]}_n

NUC-27: {[Ba₃Zn₄(TDP)₂(HCO₂)₂(OH₂)₂]·7DMF·4H₂O}_n

NUC-21: {[[(CH₃)₂NH₂]₂[CaZn(TDP)(H₂O)]·3DMF·3H₂O}_n

NUC-30: {[ZnHo(TDP)(H₂O)]·5H₂O·3DMF}_n

NUC-51: {[[(CH₃)₂NH₂]₂[BaZn(TDP)(H₂O)]·DMF·5H₂O}_n

Table S5. The molecular sizes of epoxides and corresponding products of cycloaddition reaction.

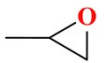
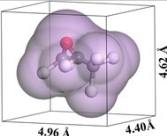
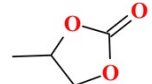
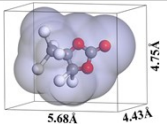
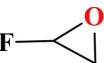
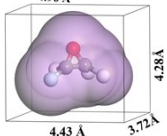
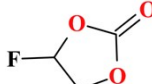
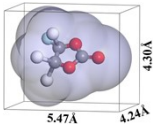
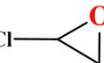
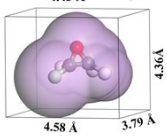
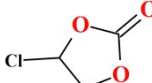
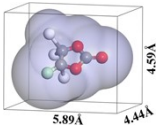
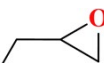
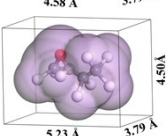
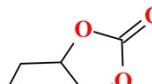
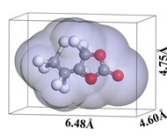
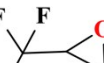
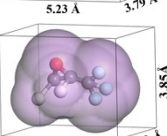
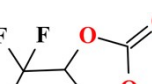
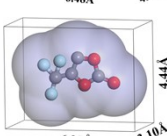
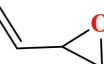
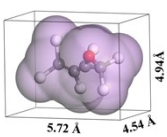
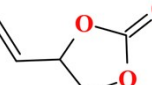
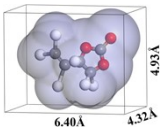
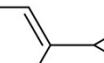
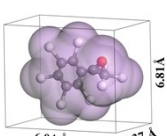
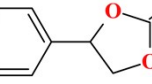
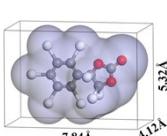
Entry	Epoxide	Epoxide size	Product	Product size
1				
2				
3				
4				
5				
6				
7				

Table S6. The molecular sizes of reactants and corresponding products of deacetalization-Knoevenagel condensation reaction.

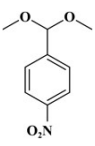
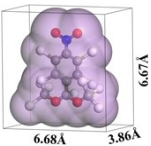
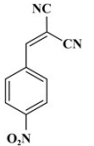
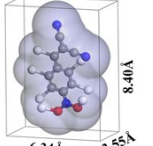
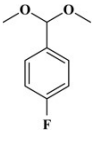
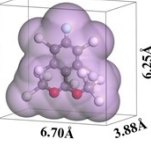
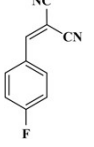
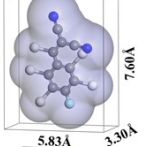
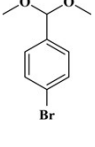
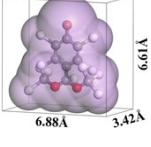
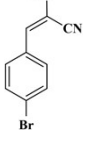
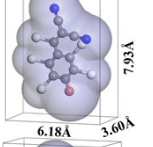
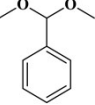
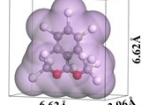
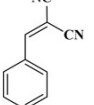
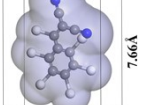
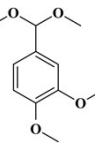
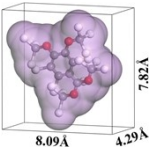
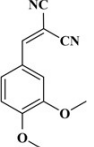
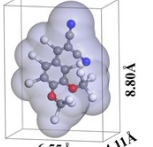
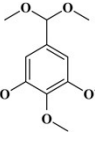
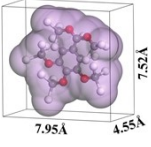
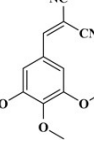
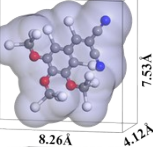
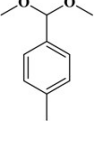
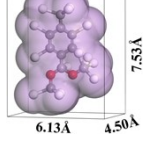
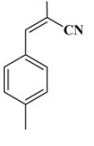
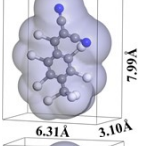
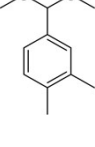
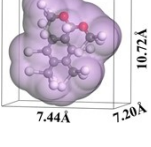
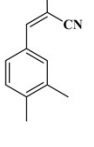
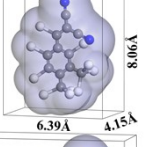
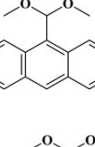
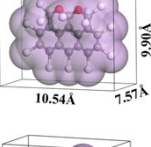
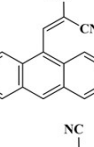
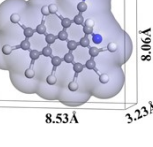
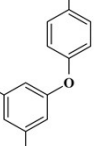
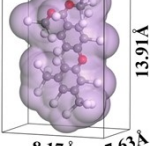
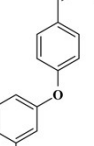
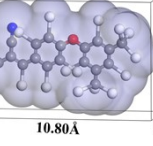
Entry	Substrate	Molecular size	Product	Product size
1		 6.68Å 3.86Å 6.67Å		 8.40Å 6.34Å 3.55Å
2		 6.70Å 3.88Å 6.25Å		 7.60Å 5.83Å 3.50Å
3		 6.61Å 3.42Å 6.68Å		 7.93Å 6.18Å 3.60Å
4		 6.62Å 3.96Å 6.62Å		 7.66Å 6.17Å 3.33Å
5		 7.82Å 4.29Å 8.09Å		 8.80Å 6.55Å 4.11Å
6		 7.52Å 4.55Å 7.95Å		 7.53Å 8.26Å 4.12Å
7		 7.53Å 4.50Å 6.13Å		 7.99Å 6.31Å 3.10Å
8		 10.72Å 7.44Å 7.20Å		 8.06Å 6.39Å 4.15Å
9		 9.90Å 10.54Å 7.57Å		 8.06Å 8.53Å 3.23Å
10		 13.91Å 8.17Å 7.63Å		 6.68Å 10.80Å 4.11Å

Table S7. The elemental analysis results of cation exchange between tetrabutylammonium cations (TBA⁺) and dimethylamine cations (DMA⁺) in **NUC-51a**.

Sample	C/%	H/%	N/%
$\{[(\text{CH}_3)_2\text{NH}_2]_2[\text{BaZn}(\text{TDP})]\}_n$ (NUC-51a)	46.18	2.94	4.90
Recovered sample of NUC-51a	58.26	6.47	3.49
$\{[(\text{C}_4\text{H}_9)_4\text{N}]_2[\text{BaZn}(\text{TDP})]\}_n$	58.47	6.68	3.35
Speculated molecular formula after complete cation exchange			

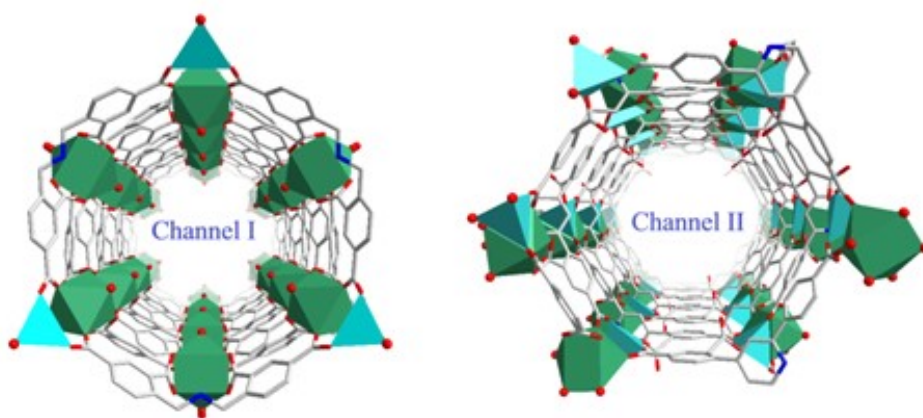


Fig. S1 The inner surface environment of cylindrical channel (a) and hexagon channel (b) in NUC-51.

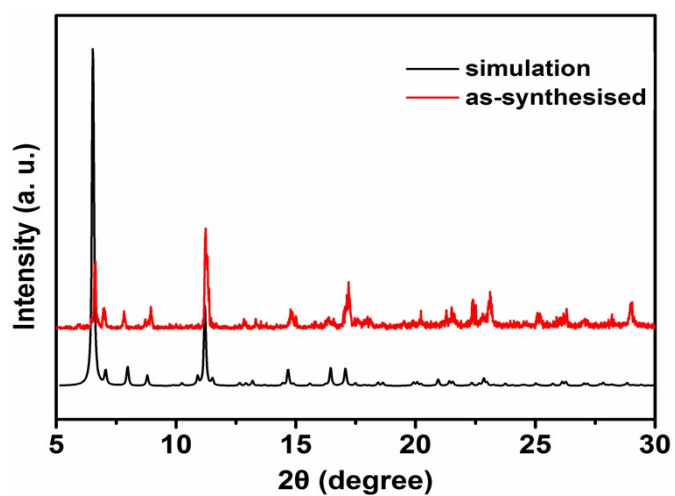


Fig. S2 The PXRD patterns of as-synthesized NUC-51 and simulation.

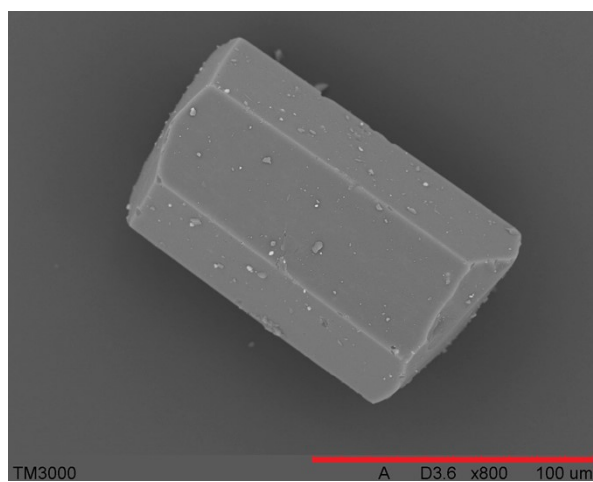


Fig. S3 The SEM imagine of NUC-51.

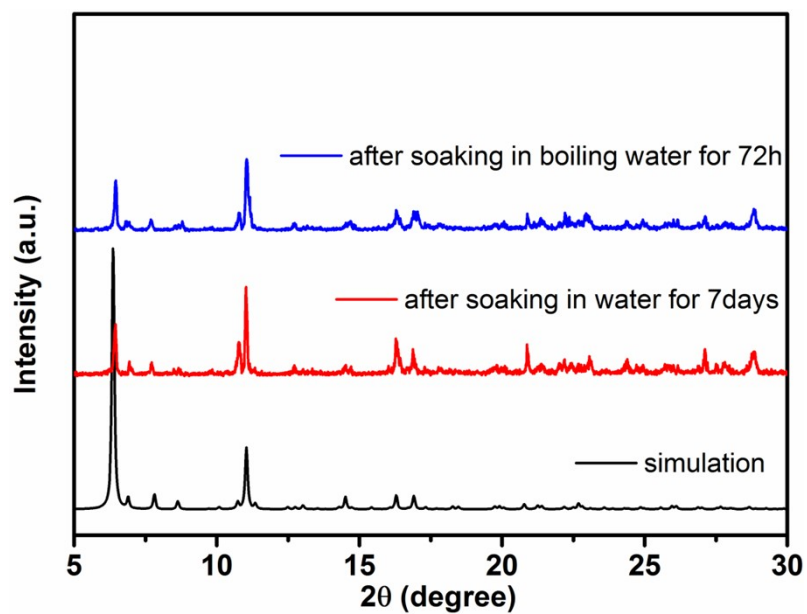


Fig. S4 The PXRD patterns of NUC-51 sample under water treatment.

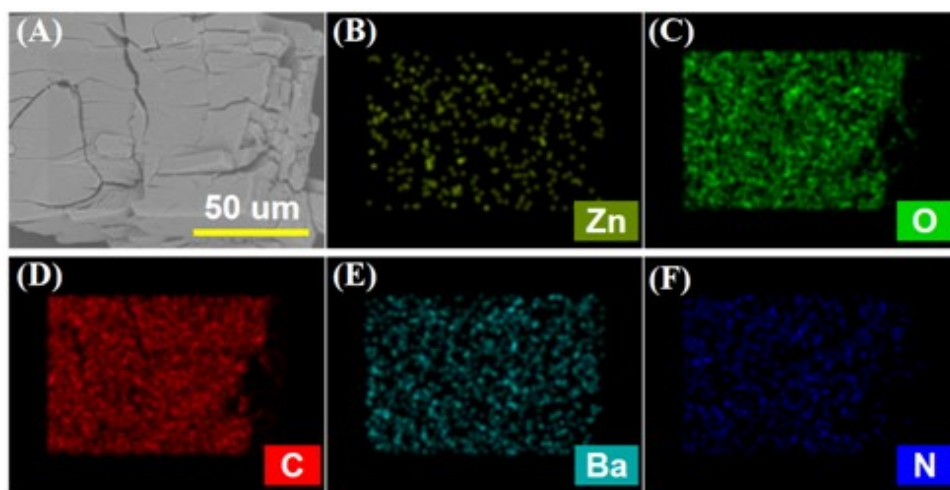


Fig. S5 Energy dispersive spectroscopy (EDS) elemental mappings of NUC-51 sample for C, N, O, Ba and Zn.

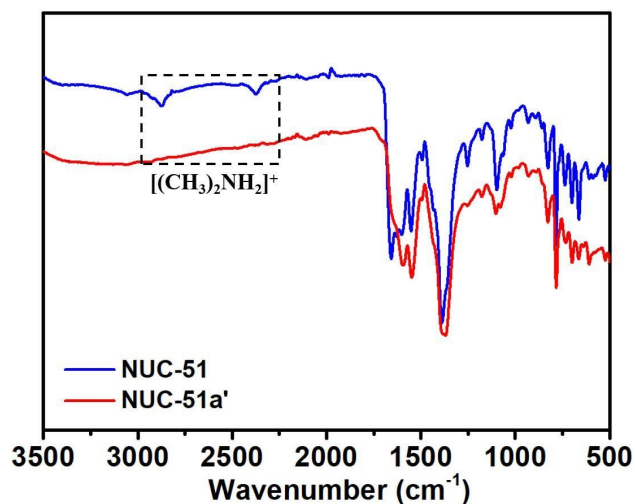


Fig. S6 The FT-IR spectrum of NUC-51 and NUC-51a'.

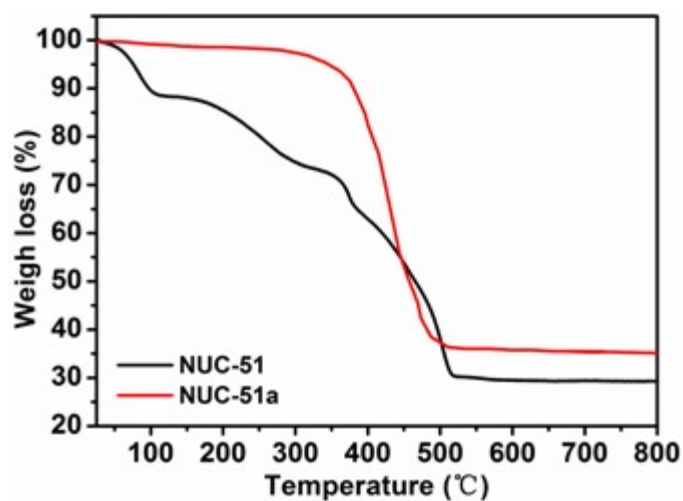


Fig. S7 The TGA curves of NUC-51 and NUC-51a.

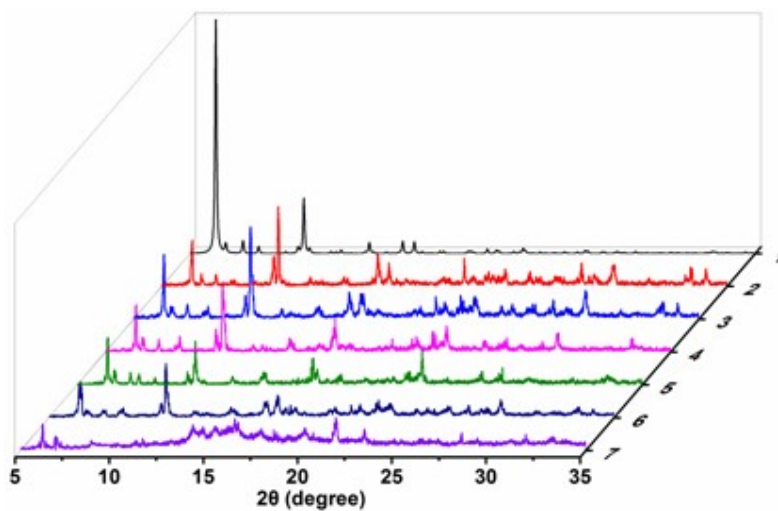


Fig. S8 The PXRD patterns of NUC-51 at variable temperatures and 1-7 correspond to simulation, 30°C, 100°C, 150°C, 280°C, 300°C and 350°C respectively.

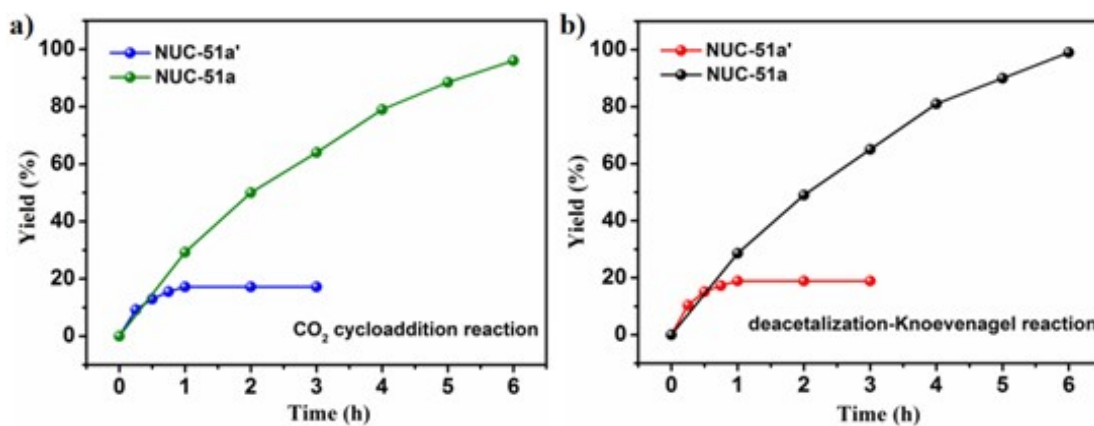


Fig. S9 The catalytic efficiency of NUC-51a and NUC-51a' for cycloaddition reaction (a) and deacetalization-Knoevenagel condensation reaction (b).

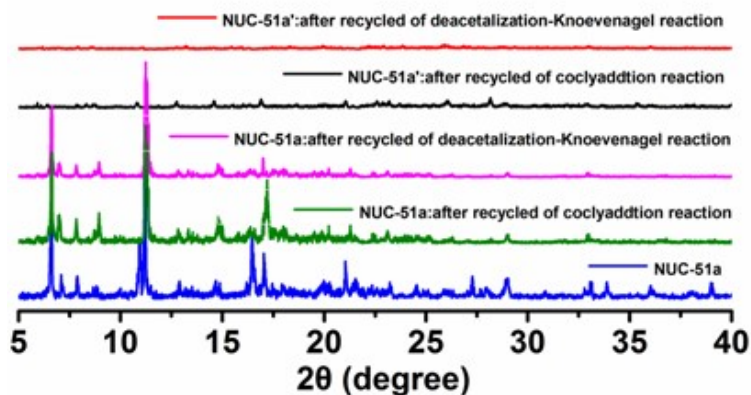


Fig. S10 The PXRD patterns of NUC-51a and NUC-51a' after cycloaddition reaction and deacetalization-Knoevenagel condensation reaction.

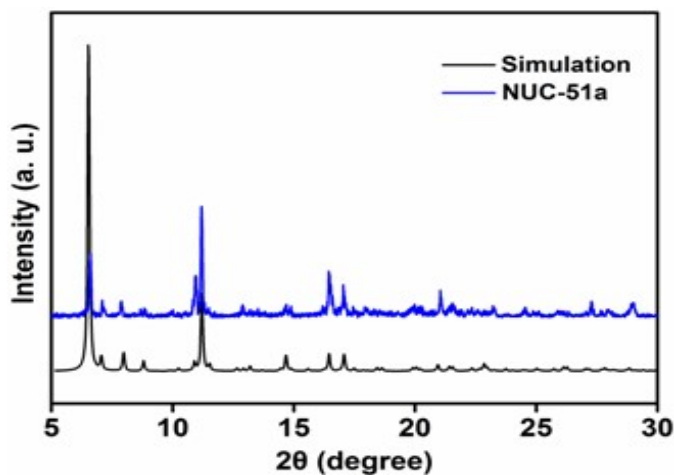


Fig. S11 The PXRD patterns of NUC-51a and simulation.

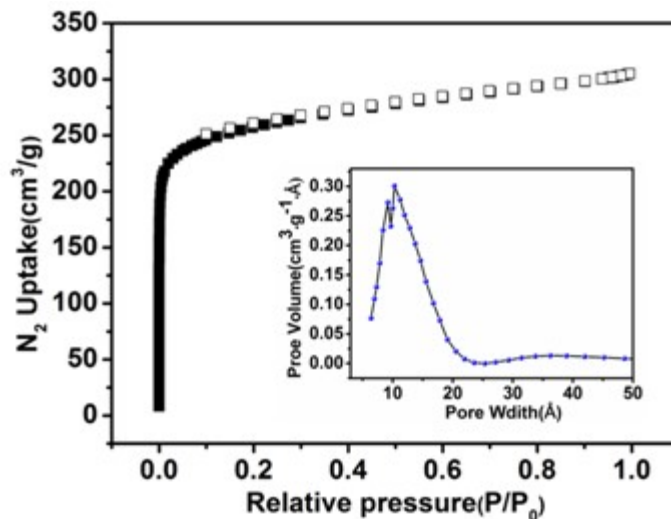


Fig. S12 N₂ adsorption and desorption isotherms of NUC-51a at 77 K.

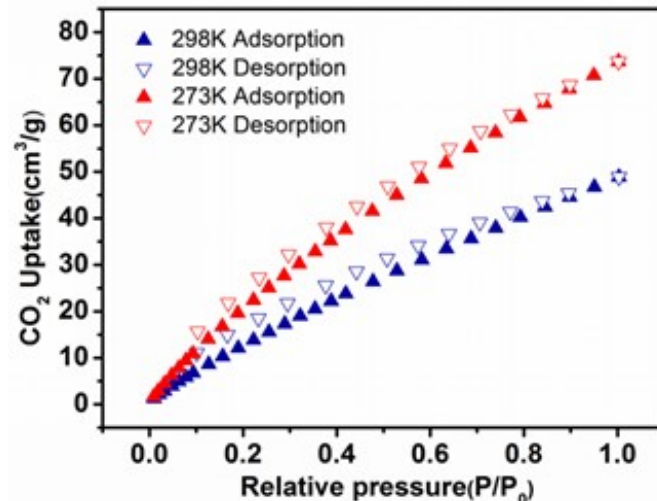


Fig. S13 CO₂ sorption isotherms of NUC-51a at 273 and 298 K.

Isosteric Heat Calculation.

The Q_{st} value is a parameter that describes the average enthalpy of adsorption for an adsorbing gas molecule at a specific surface coverage and is usually evaluated using two or more adsorption isotherms collected at similar temperatures. The zero-coverage isosteric heat of adsorption is evaluated by first fitting the temperature-dependent isotherm data to a virial-type expression, which can be written as:

$$\ln p = \ln N + \frac{1}{T} \sum_{i=0}^m a_i N^i + \sum_{j=0}^n b_j N^j$$

N: Adsorption capacity (mg/g); **p**: Pressure (mmHg); **T**: Temperature (K); **a_i** · **b_j**: Empirical constant; **R**: Universal gas constant (8.314 J·mol⁻¹·K⁻¹)

The isosteric enthalpy of adsorption (Q_{st}):

$$Q_{st} = -R \sum_{i=0}^m a_i N^i$$

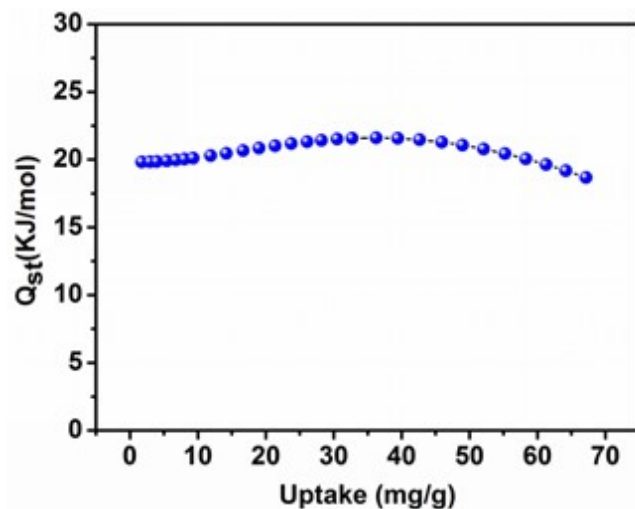


Fig. S14 CO₂ adsorption heat calculated by the virial equation of NUC-51a.

Yield Calculation Based on the GC-MS Analysis

Gas chromatography mass spectrometry (GC-MS) analyses were executed on a time-of-flight Thermo Fisher Trace ISQ GC/MS instrument, the yield (%) was calculated based on the consumption of starting material using the equation:

$$\text{Yield (\%)} = \left(\frac{\frac{\text{area of reactant at 0 hour}}{\text{area of internal standard at 0 hour}} - \frac{\text{area of reactant at any time}}{\text{area of internal standard at any time}}}{\frac{\text{area of reactant at 0 hour}}{\text{area of internal standard at 0 hour}}} \right)$$

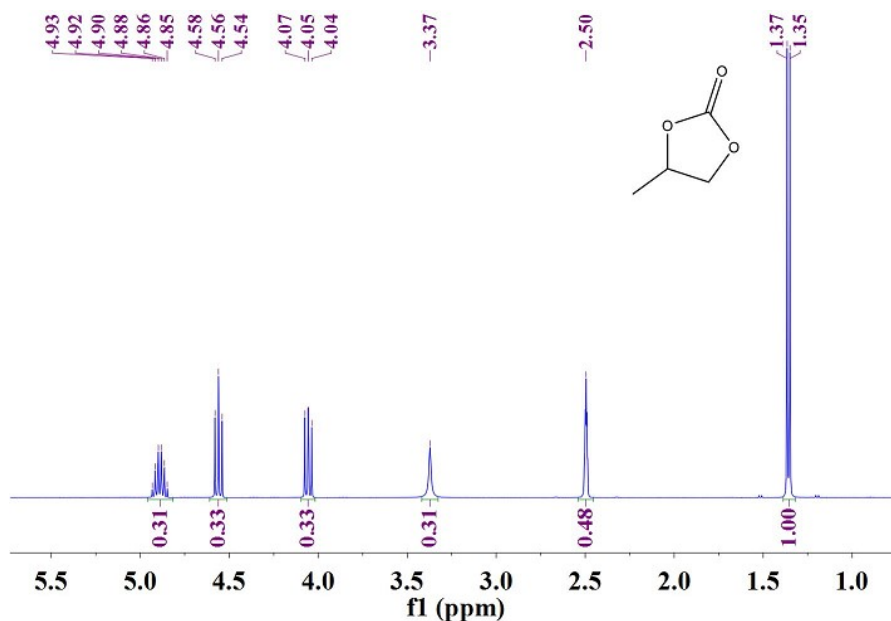


Fig. S15 ¹H NMR spectrum of propylene carbonate.

δ H (400 MHz, DMSO) 4.96-4.82 (0 H, m), 4.56 (0 H, t, J 8.0), 4.10-4.02 (0 H, m), 1.36 (1 H, d, J 6.2).

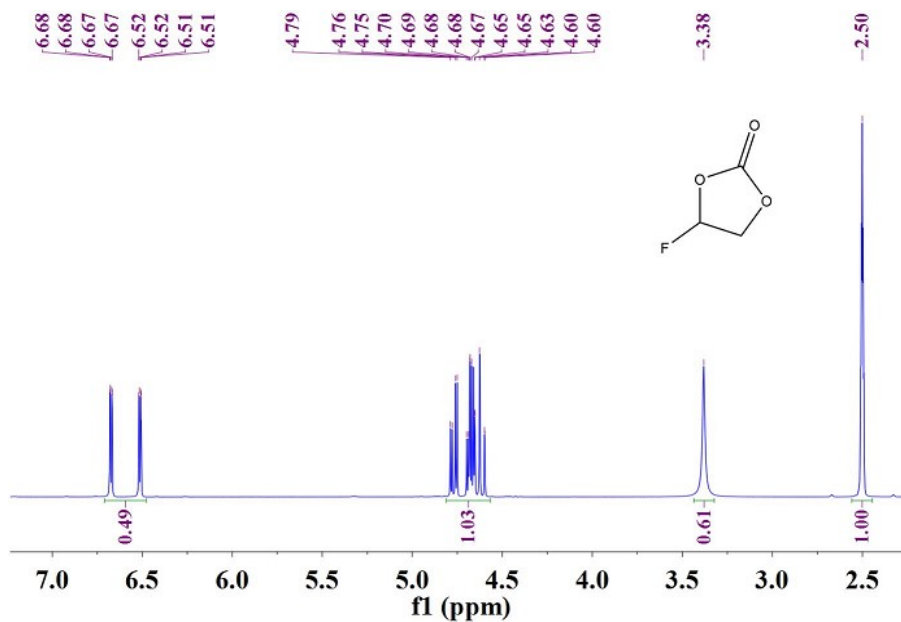


Fig. S16 ^1H NMR spectrum of 4-fluoro-1,3-dioxolan-2-one.

δ H (400 MHz, DMSO) 6.59 (0 H, ddd, J 64.4, 4.1, 0.9), 4.81-4.57 (1 H, m), 3.38 (1 H, s), 2.50 (1 H, s).

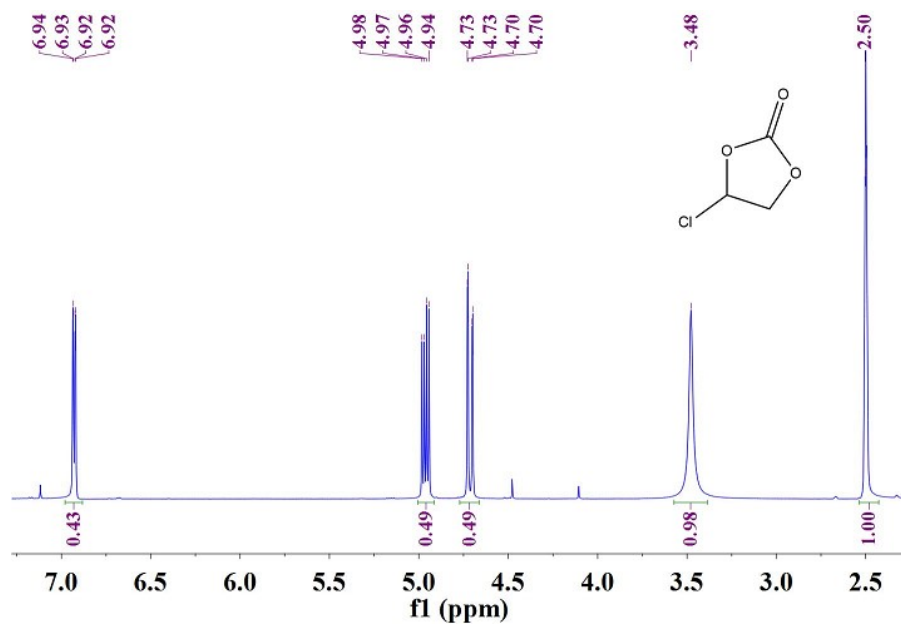


Fig. S17 ^1H NMR spectrum of 4-chloro-1,3-dioxolane-2-one.

δ H (400 MHz, DMSO) 6.93 (0 H, dd, J 5.3, 1.3), 4.96 (0 H, dd, J 10.5, 5.3), 4.71 (0 H, dd, J 10.5, 1.3), 3.48 (1 H, s), 2.50 (1 H, s).

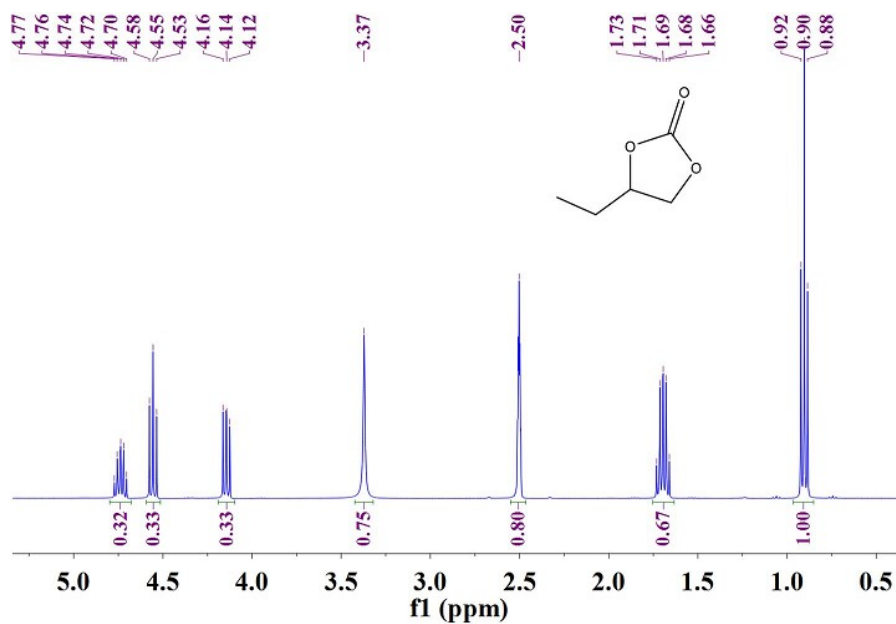


Fig. S18 ^1H NMR spectrum of 4-ethyl-1,3-dioxolan-2-one.

δ H (400 MHz, DMSO) 4.80 - 4.68 (0 H, m), 4.55 (0 H, t, J 8.1), 4.19-4.10 (0 H, m), 3.37 (1 H, s), 2.50 (1 H, s), 1.75-1.63 (1 H, m), 0.90 (1 H, t, J 7.4).

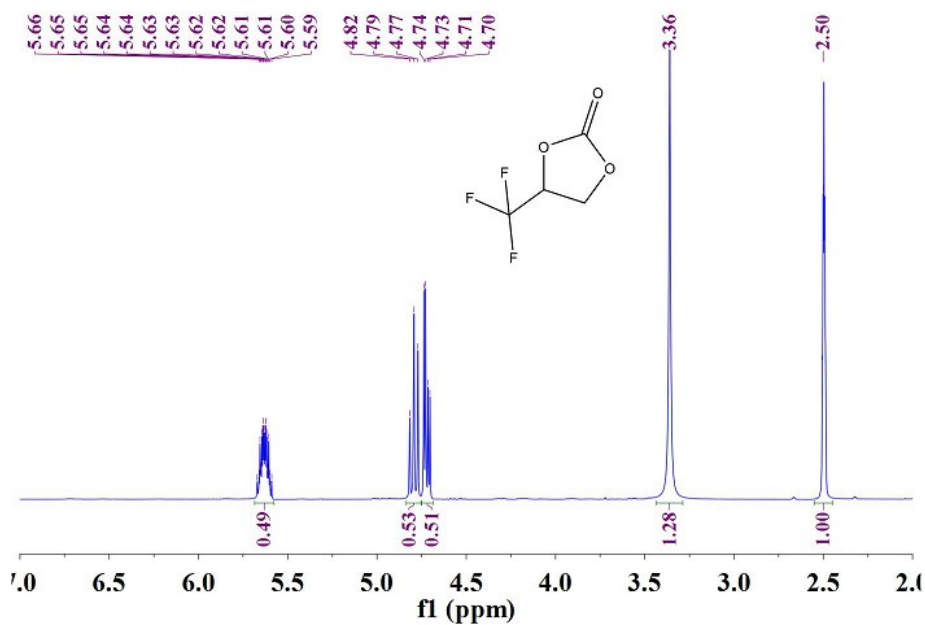


Fig. S19 ^1H NMR spectrum of 4-(trifluoro)-1,3-dioxolane-2-one.

δ H (400 MHz, DMSO) 5.69-5.58 (0 H, m), 4.79 (1 H, t, J 9.1), 4.72 (1 H, dd, J 9.7, 4.1), 3.36 (1 H, s), 2.50 (1 H, s).

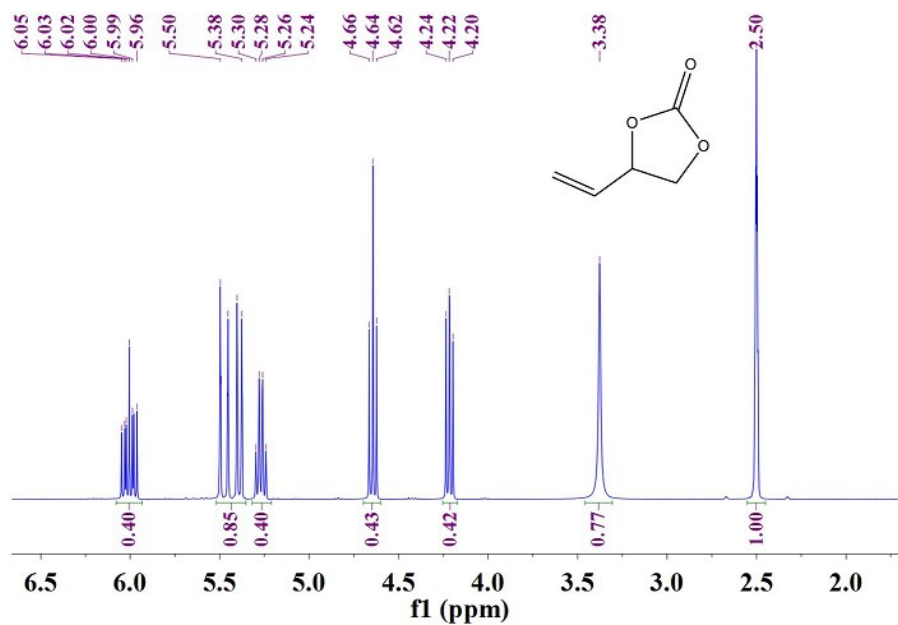


Fig. S20 ^1H NMR spectrum of 4-vinyl-1,3-dioxolan-2-one.

δ H (400 MHz, DMSO) 6.08-5.93 (0 H, m), 5.43 (1 H, dd, J 34.1, 13.8), 5.27 (0 H, q, J 7.2), 4.64 (0 H, t, J 8.2), 4.25-4.17 (0 H, m), 3.38 (1 H, s), 2.50 (1 H, s).

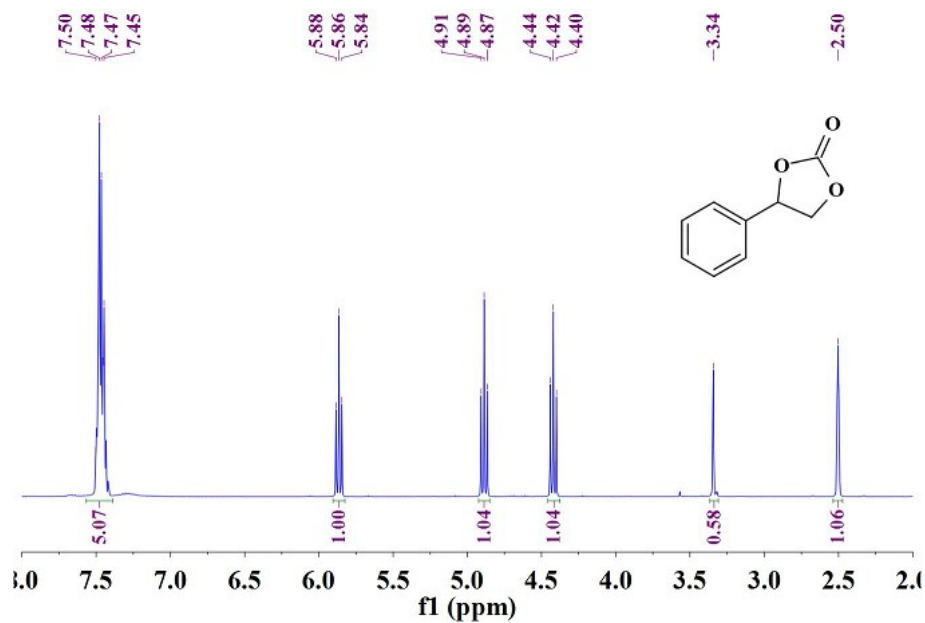


Fig. S21 ^1H NMR spectrum of 4-phenyl-1,3-dioxolan-2-one.

δ H (400 MHz, DMSO) 7.57-7.39 (5 H, m), 5.86 (1 H, t, J 8.0), 4.89 (1 H, t, J 8.3), 4.42 (1 H, t, J 8.2), 3.34 (1 H, s), 2.50 (1 H, s).

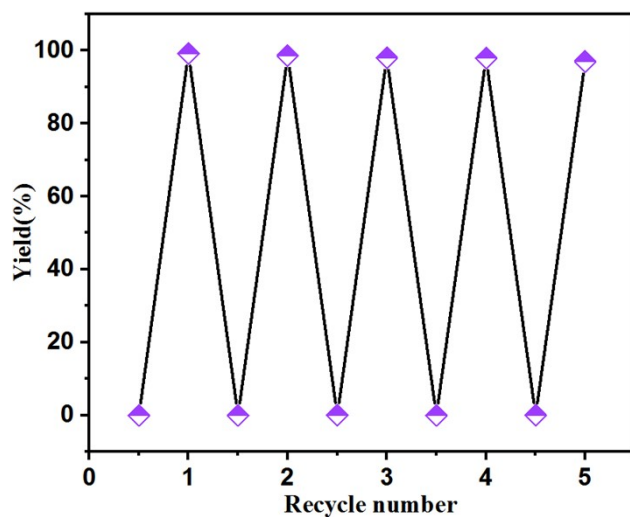


Fig. S22 Recyclability study (five cycles) for catalytic activities of **NUC-51a** in cycloaddition reaction of styrene oxide with CO_2 .

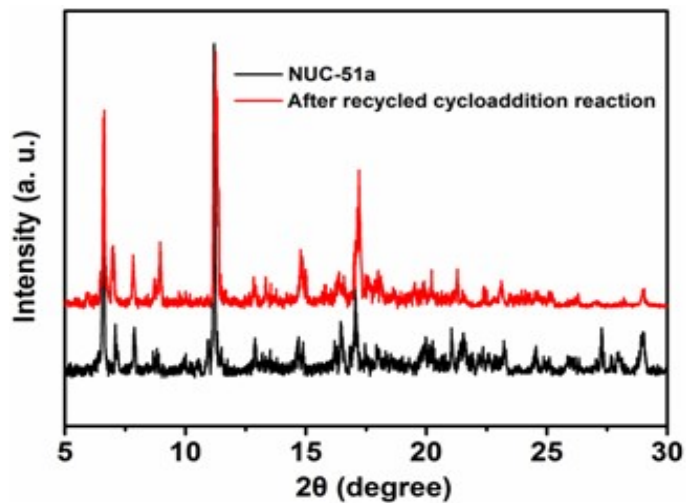


Fig. S23 The PXRD patterns of **NUC-51a** after recycled cycloaddition reaction.

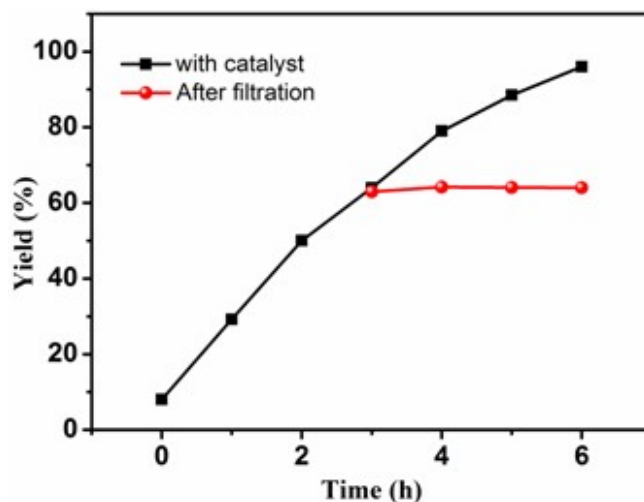


Fig. S24 Evidence of heterogeneous nature of **NUC-51a** in the cycloaddition reaction.

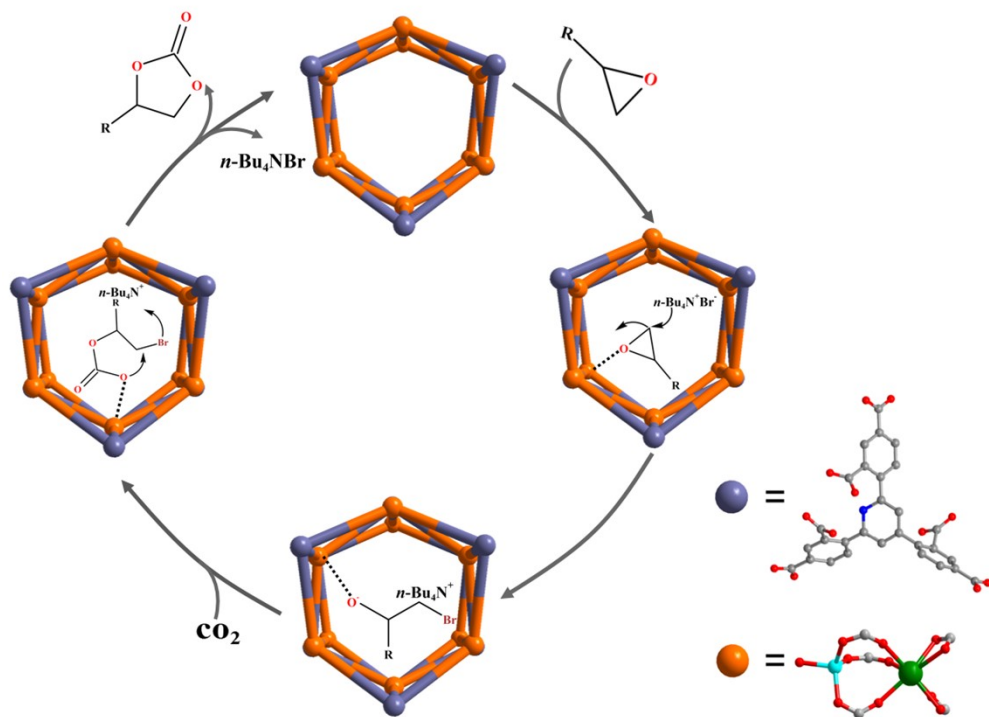


Fig. S25 The catalytic mechanism of cycloaddition reaction of epoxides with CO₂.

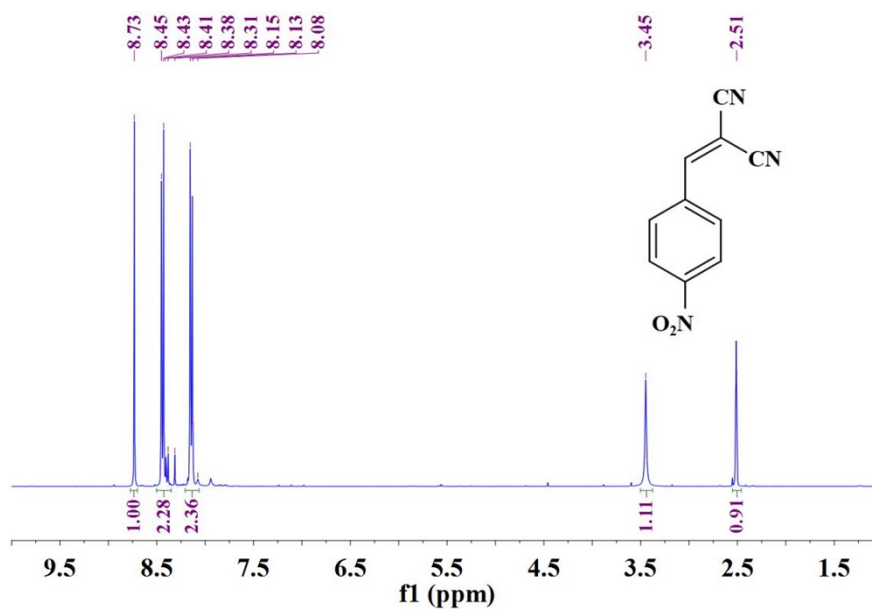


Fig. S26 ¹H NMR spectrum of 2-[(4-nitrophenyl) methylene] propanedinitrile.

δ H (400 MHz, DMSO) 8.73 (1 H, s), 8.42 (2 H, dd, J 17.3, 10.4), 8.25-8.06 (2 H, m), 3.45 (1 H, s), 2.51 (1 H, s).

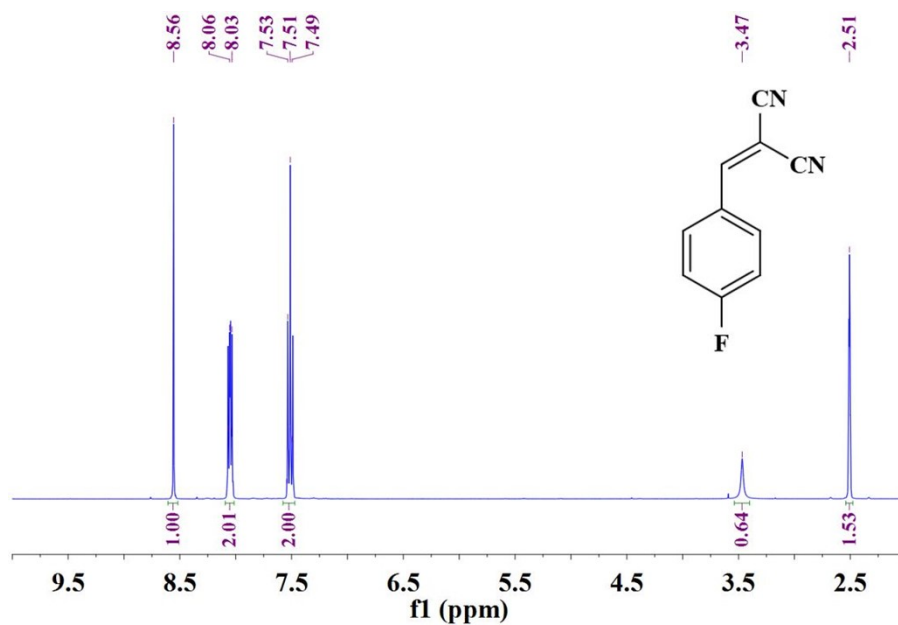


Fig. S27 ^1H NMR spectrum of 2-[(4-fluorophenyl)methylidene] propanedinitrile.

δ H (400 MHz, DMSO) 8.56 (1 H, s), 8.15-8.00 (2 H, m), 7.51 (2 H, t, J 7.8), 3.47 (1 H, s), 2.51 (2 H, s).

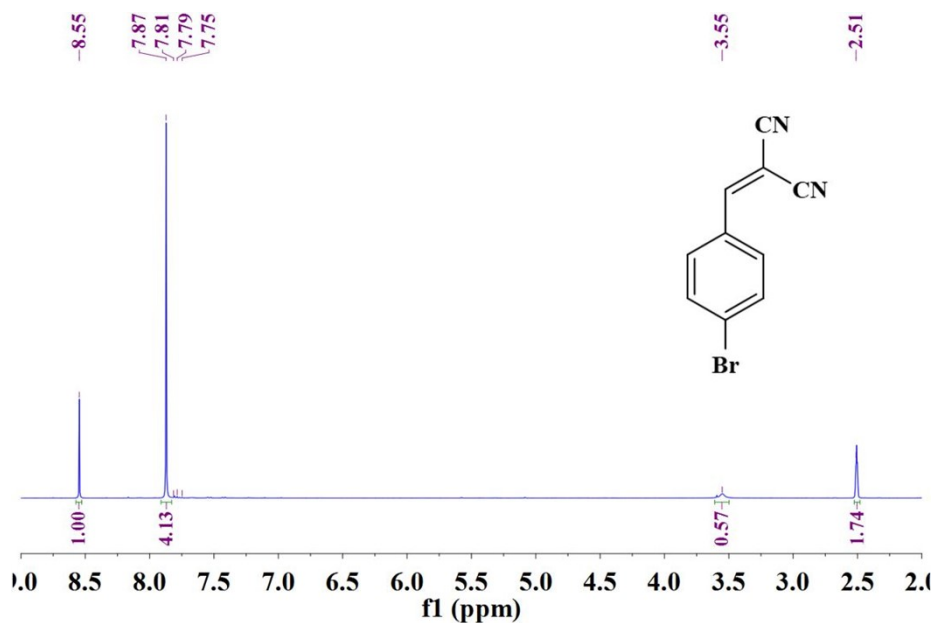


Fig. S28 ^1H NMR spectrum of 2-[(4-bromophenyl)methylidene] propanedinitrile.

δ H (400 MHz, DMSO) 8.55 (1 H, s), 7.87 (4 H, s), 3.55 (1 H, s), 2.51 (2 H, s).

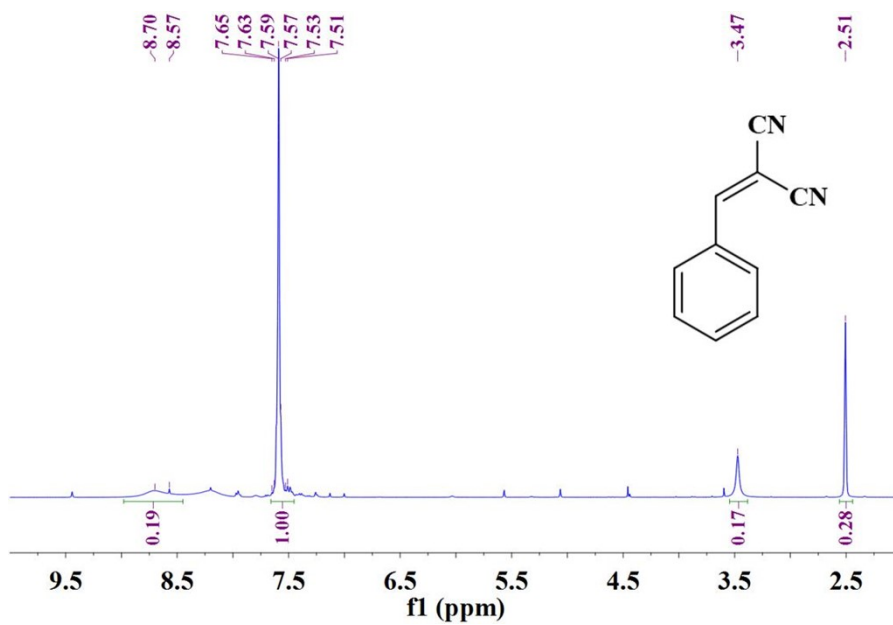


Fig. S29 ^1H NMR spectrum of 2-(phenylmethylidene)propanedinitrile.

δ H (400 MHz, DMSO) 8.63 (1 H, d, J 52.0), 7.66-7.46 (5 H, m), 3.47 (1 H, s), 2.51 (1 H, s).

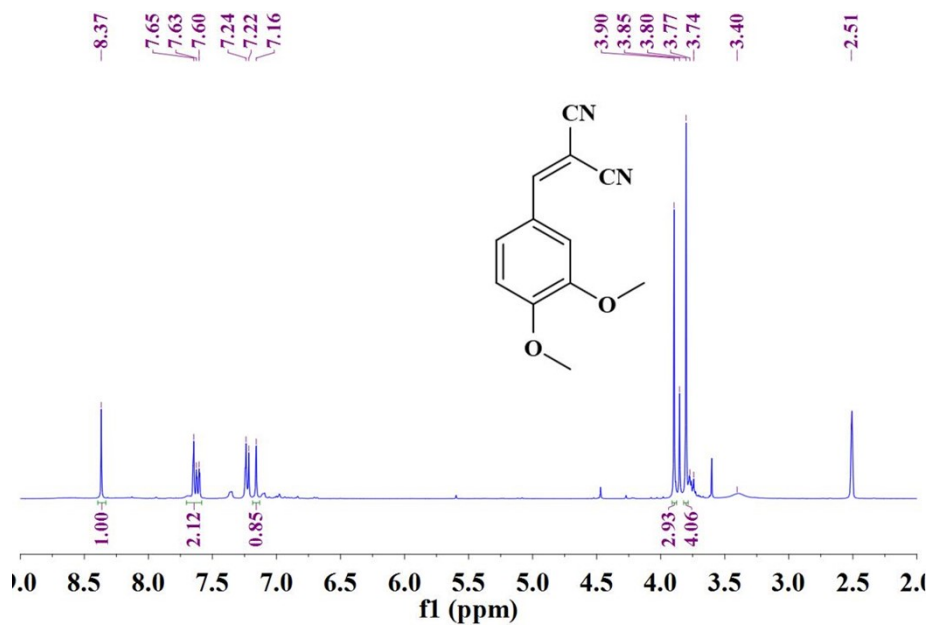


Fig. S30 ^1H NMR spectrum of 2-[(3,4-dimethoxyphenyl)methylidene]propanedinitrile.

δ H (400 MHz, DMSO) 8.37 (1 H, s), 7.70-7.58 (2 H, m), 7.25-7.13 (2 H, m), 3.90 (3 H, s), 3.82-3.74 (5 H, m), 2.51 (2 H, s).

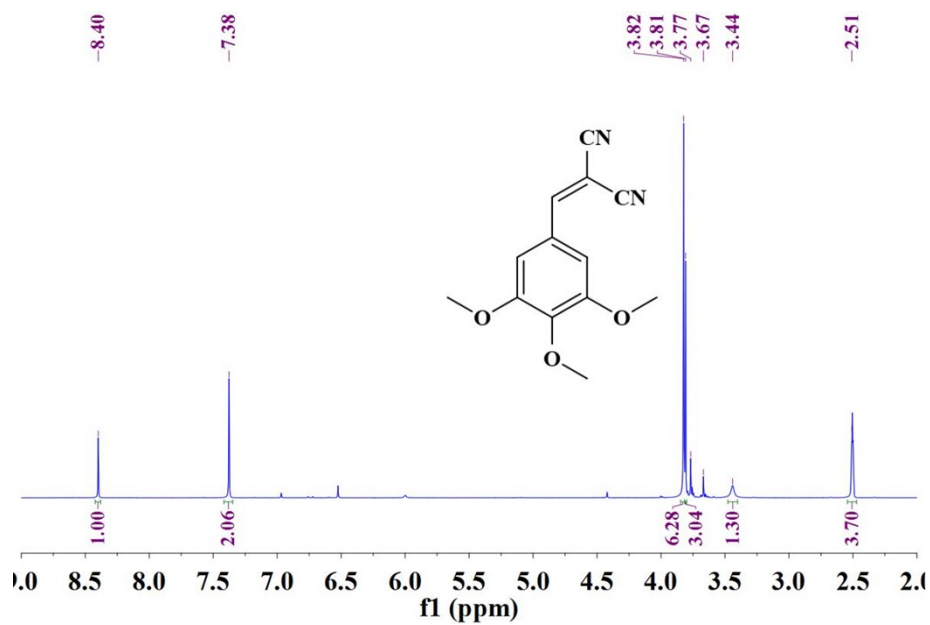


Fig. S31 ^1H NMR spectrum of 2-[(3,4,5-trimethoxyphenyl)methylidene]propanedinitrile.

δ H (400 MHz, DMSO) 8.40 (1 H, s), 7.38 (2 H, s), 3.83 (1 H, s), 3.81 (3 H, s), 3.44 (1 H, s), 2.51 (4 H, s).

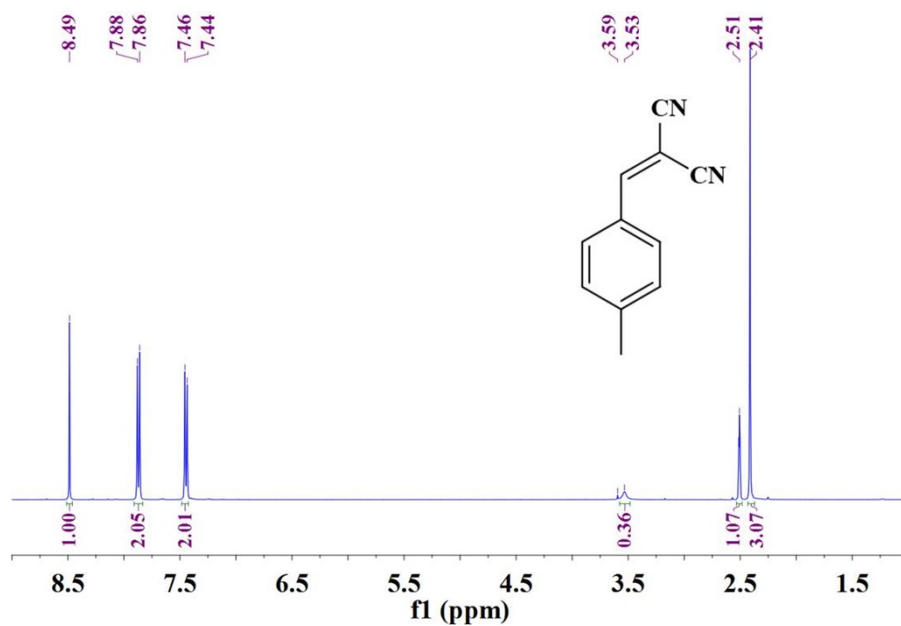


Fig. S32 ^1H NMR spectrum of 2-[(4-methylphenyl)methylidene]propanedinitrile.

δ H (400 MHz, DMSO) 8.49 (1 H, s), 7.87 (2 H, d, J 8.3), 7.45 (2 H, d, J 8.1), 3.56 (0 H, d, J 24.4), 2.51 (1 H, s), 2.41 (3 H, s).

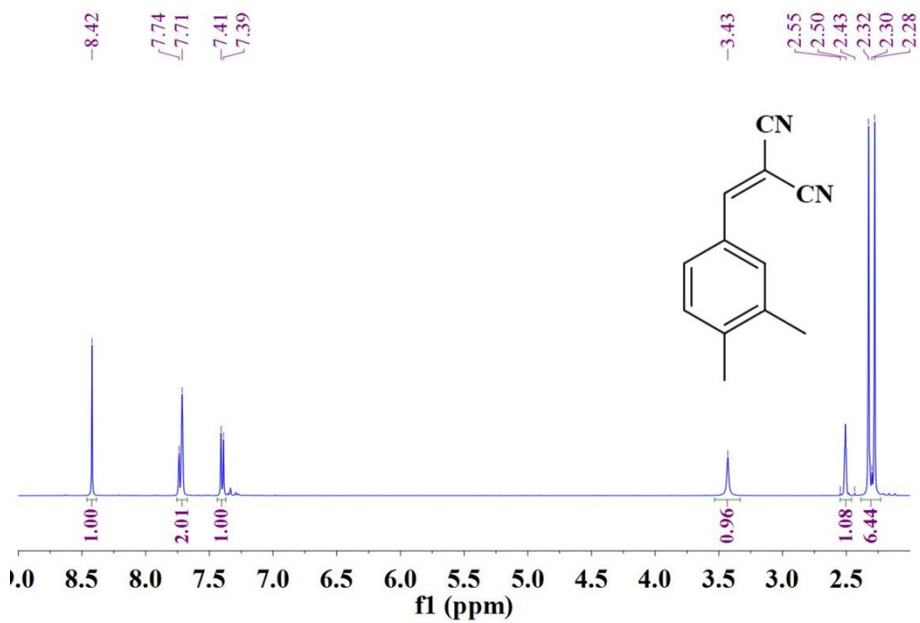


Fig. S33 ^1H NMR spectrum of 2-[(3,4-dimethylphenyl)methylidene]propanedinitrile.

δ H (400 MHz, DMSO) 8.42 (1 H, s), 7.73 (2 H, d, J 9.5), 7.40 (1 H, d, J 7.8), 3.43 (1 H, s), 2.52 (1 H, d, J 17.5), 2.40-2.21 (6 H, m).

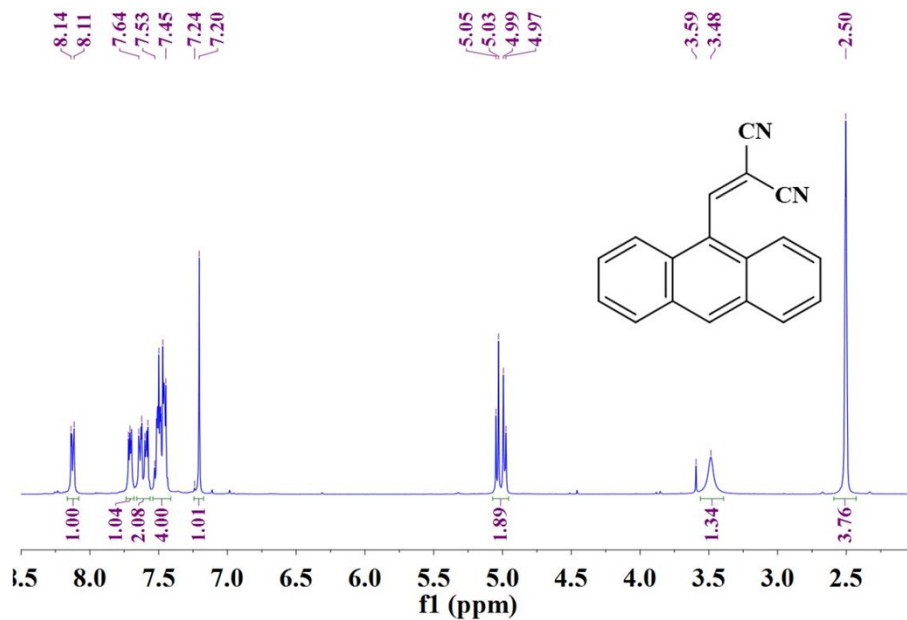


Fig. S34 ^1H NMR spectrum of 2-[(anthracen-9-yl)methylidene]propanedinitrile.

δ H (400 MHz, DMSO) 8.13 (1 H, d, J 8.9), 7.74-7.68 (1 H, m), 7.61 (2 H, dd, J 18.0, 8.8), 7.54-7.41 (4 H, m), 7.22 (1 H, d, J 13.6), 5.01 (2 H, dd, J 21.5, 7.4), 3.48 (1 H, s), 2.50 (4 H, s).

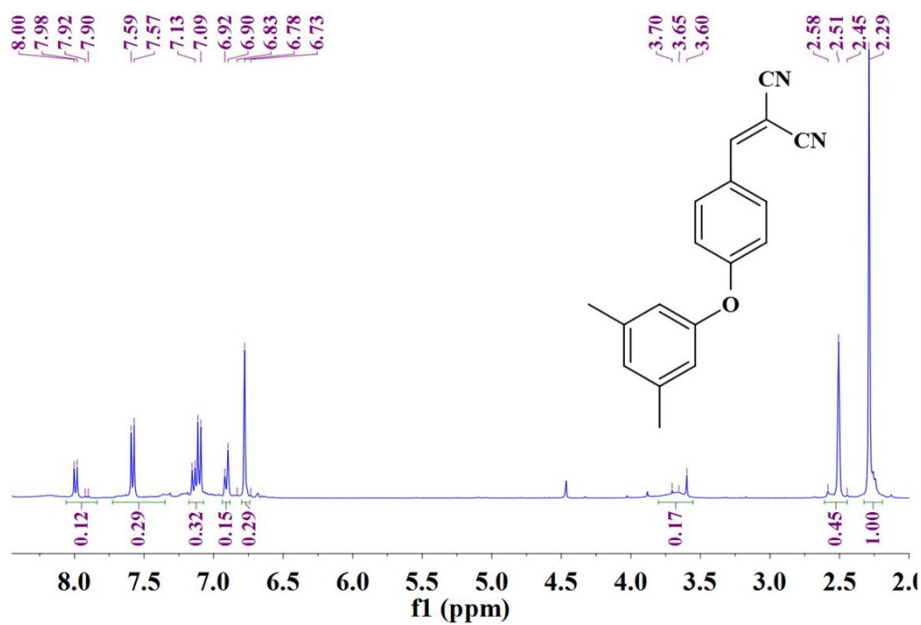


Fig. S35 ^1H NMR spectrum of 2-[[4-(3,5-dimethylphenoxy)phenyl]methylidene]propanedinitrile.

δ H (400 MHz, DMSO) 7.95 (0 H, dd, J 32.0, 8.7), 7.58 (0 H, d, J 8.7), 7.12 (0 H, dd, J 16.7, 8.7), 6.91 (0 H, d, J 8.9), 6.84-6.73 (0 H, m), 3.84- 3.54 (0 H, m), 2.61- 2.44 (0 H, m), 2.29 (1 H, s).

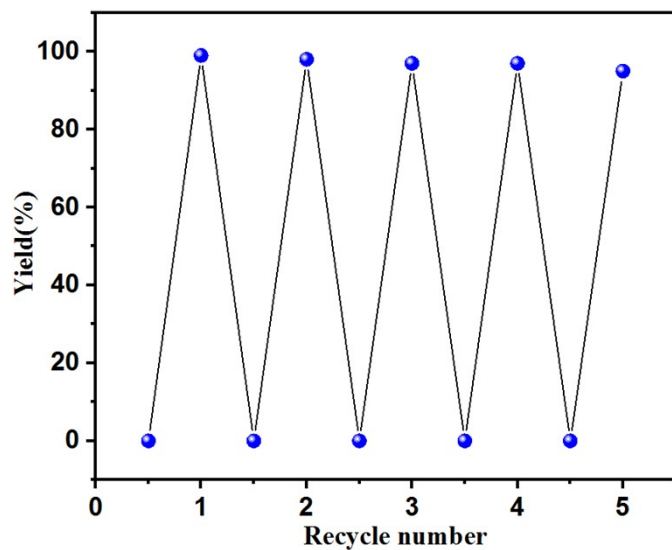


Fig. S36 Recyclability study for catalytic activities of NUC-51a in deacetalization-Knoevenagel reaction.

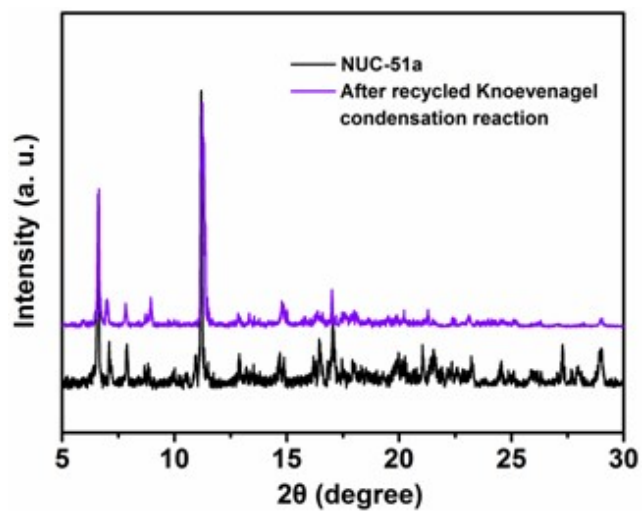


Fig. S37 The PXRD patterns of NUC-51a after recycled deacetalization-Knoevenagel reaction.

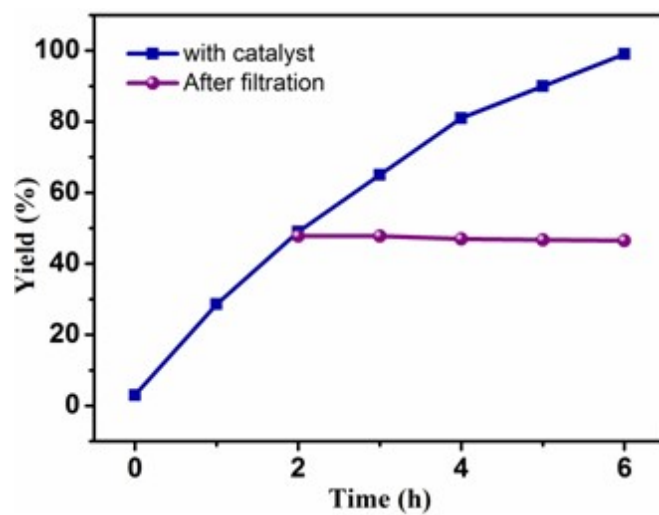


Fig. S38 Evidence of heterogeneous nature of NUC-51a in the deacetalization-Knoevenagel reaction.

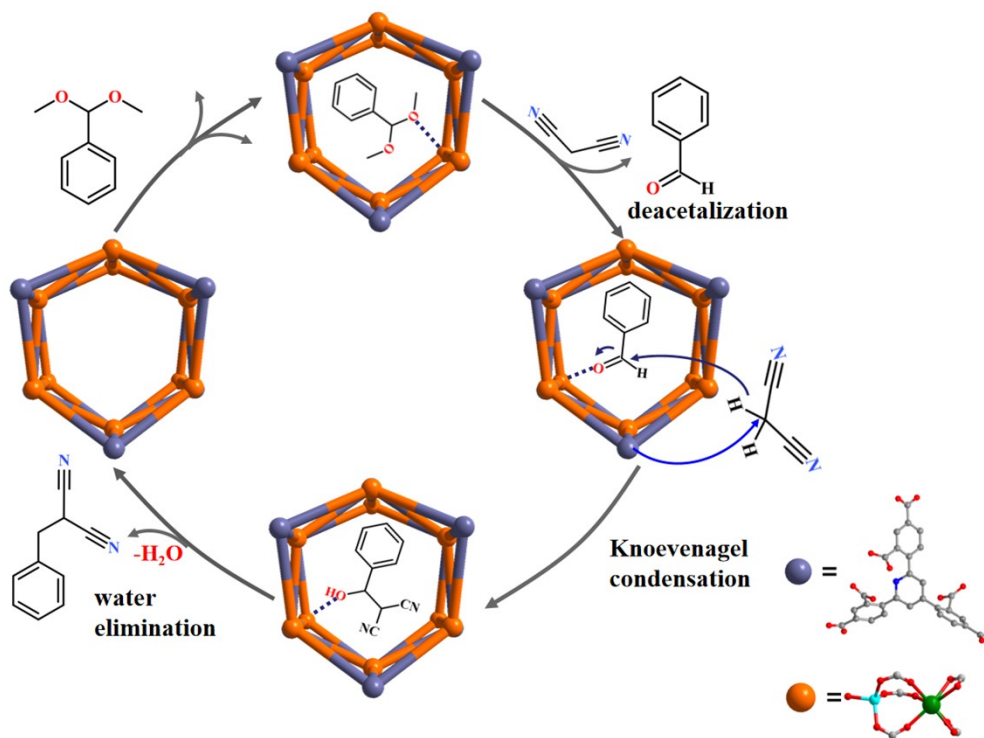


Fig. S39 Plausible reaction mechanism of deacetalization-Knoevenagel reaction catalyzed by NUC-51a.

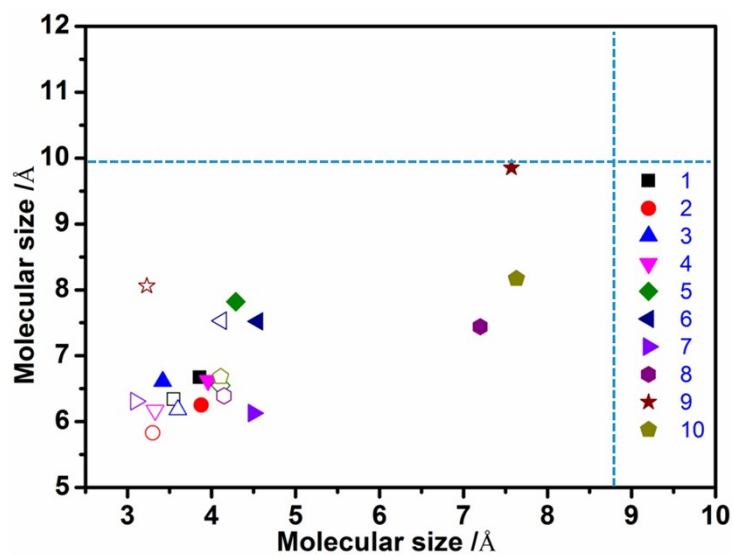


Fig. S40 Two dimensional molecular sizes of deacetalization-Knoevenagel reaction reactants (close symbol) and products (open symbol) simulated by Mater Studio (The two-dimensional molecular sizes refer to the smaller two of the three parameters of molecular length, width and height).

Reference:

- S1.** Y. B. N. Tran.; Phuong T. K. Nguyen.; Quang T. Luong, Khoi D. Nguyen. Series of M-MOF-184 (M = Mg, Co, Ni, Zn, Cu, Fe) Metal-Organic Frameworks for Catalysis Cycloaddition of CO₂. *Inorg. Chem.*, 2020, **59**, 16747-16759.
- S2.** Rachuri, Y.; Kurisingal, J. F.; Chitumalla, R. K.; Vuppala, S.; Gu, Y.; Jang, J.; Choe, Y.; Syresh, E.; Pare, D. Adenine-based Zn(II)/Cd(II) metal-organic frameworks as efficient heterogeneous catalysts for facile CO₂ fixation into cyclic carbonates: a DFT-supported study of the reaction mechanism. *Inorg. Chem.*, 2019, **58**, 11389-11403.
- S3.** Li, X. Y.; Ma, L. N.; Liu, Y.; Lei, H.; Zhu, Z. Honeycomb Metal-Organic Framework with Lewis Acidic and Basic Bifunctional Sites: selective adsorption and CO₂ catalytic fixation. *ACS Appl. Mater. Interfaces.*, 2018, **10**, 10965-10973.
- S4.** Patel, P.; Parmar, B.; Kureshy, R. I.; Khan, N. H.; Suresh, E. Amine-Functionalized Zn(II) MOF as an Efficient Multifunctional Catalyst for CO₂ Utilization and Sulfoxidation Reaction. *Dalton Trans.*, 2018, **47**, 8041-8051.
- S5.** Chen, H.; Fan, L.; Hu, T.; Zhang, X. 6s-3d {Ba₃Zn₄}-Organic Framework as an effective heterogeneous catalyst for chemical fixation of CO₂ and knoevenagel condensation reaction. *Inorg. Chem.*, 2021, **60**, 3384-3392.
- S6.** Chen, H.; Fan, L.; Zhang, X. Highly robust 3s-3d {CaZn}-Organic Framework for excellent catalytic performance on chemical fixation of CO₂ and knoevenagel condensation reaction. *ACS Appl. Mater. Interfaces*, 2020, **12**, 54884-54892.
- S7.** Zhang, T.; Chen, H.; Lv, H.; Li, Q.; Zhang, X. Nanochannel-based heterometallic {Zn^{II}Ho^{III}}-organic framework with high catalytic activity for the chemical fixation of CO₂. *RSC Adv.*, 2021, **11**, 9731-9739.